Failure of Rocks in the Laboratory and in the Earth

J.W. Rudnicki

Northwestern University, Evanston, IL USA
jwrudn@northwestern.edu

1 Introduction

Although rocks, at least some of them, are nearly as old as the Earth itself, their behaviour continues to play an important role in a variety of applications and phenomena of societal interest. These include natural disasters, such as landslides, volcanic eruptions and earthquakes. Rocks are widely used for building materials, foundations, tunnels and underground facilities. Most of the world's energy now, and for the foreseeable future, comes from the shallow crust and an understanding of rock behaviour is essential to efficient and safe production and storage. Moreover, many of the by-products of energy production are re-injected to the shallow crust. An increasingly important application is geological sequestration of carbon dioxide, injection into the earth to mitigate harmful effects on the climate [42]. Many of these problems involve not only mechanical behaviour but also its coupling with fluid flow, heat and chemistry.

The vast majority of tests performed on rocks to determine constitutive behaviour have been on cylindrical specimens loaded axially symmetrically. Of these, most have been in axisymmetric compression (largest magnitude principal stress is compressive). There are historical and technical reasons for the emphasis on this type of test and it does provide information on the dependence of the behaviour on the mean stress (or confining stress). Such tests, however, provide very limited information about the response for the range of deviatoric stress states. Information about the full range of deviatoric stress states is needed for applications, in which the stress is seldom axially symmetric, and for numerical simulations.

A particular issue is the role of the intermediate principal stress: In axisymmetric tests it is equal to either the most or least compressive principal stress. The Mohr-Coulomb condition (e.g., [14], [29]) posits behaviour depending only on the sum and difference of the largest and smallest principal stresses and, thus, is independent of the intermediate principal stress. Mogi ([20],[21],[22]) noted, however, that the difference in the behaviour observed in axially symmetric compression and extension indicated a dependence on

the intermediate principal stress. In seminal work intended to further explore the role of the intermediate principal stress, Mogi ([21], [22]) conducted experiments in a true triaxial apparatus in which a cubical specimen could be subjected to three different principal stresses. Despite their importance, few true triaxial tests have been conducted on rocks (though there are more on soils and concrete). Recently, however, Haimson ([9], [5], [10], [24]) has fabricated a true triaxial apparatus similar in design to that of Mogi and has conducted a series of true triaxial tests on several different rock types.

This paper uses the theoretical framework of shear localization as a bifurcation from homogeneous deformation ([33], [30], [3]) to interpret observations of the inclination of the failure plane in true triaxial tests on Westerly granite. Although this theory also yields a prediction of the failure stress, assumed to coincide with shear localization, in terms of a critical value of the slope of the stress strain curve, the emphasis here is on the orientation of the failure plane. One reason is that it is difficult to determine the precise point on the stress strain curve where localization occurs. Although the zone in which failure occurs is seldom precisely planar, it is often nearly so in the central portion of the specimen and, thus, is relatively easy to observe. Depending on the deviatoric stress state, the stress at localization is predicted to be from slightly before to well after a peak in the stress strain curve. Although there is some observational evidence for these predictions, failure tends to occur closer to peak than predicted for axially symmetric stress states. This discrepancy is thought to be due to the limitations of smooth yield surface models to capture adequately the response to abrupt changes in the pattern of deformation (as must occur for localization in axisymmetric states), but these limitations do not seem to significantly affect the failure angle.

Because the theory of shear localization is strongly dependent on the type of constitutive relation used, the paper first discusses the framework for rate-independent, elastic plastic models and, especially the form for a class that depends on all three stress invariants. A particular form of yield function dependent on three invariants is used to infer parameters of the function from data on Westerly granite and use them to predict the failure angle.

2 Form of Constitutive Relation

The constitutive relation is assumed to have the standard form for a rate-independent solid. Strain increments are the sum of elastic and inelastic parts

$$d\varepsilon_{ij} = d\varepsilon^e_{ij} + d\varepsilon^p_{ij} \tag{1}$$

(and attention is restricted to small strain). The elastic portion is related to the stress increment by

$$d\varepsilon^e_{ij} = C_{ijkl} d\sigma_{kl} \tag{2}$$

where C_{ijkl} is the elastic compliance tensor. For isotropy, this is given by

$$C_{ijkl} = \frac{1}{2G}\left\{\frac{1}{2}(\delta_{ik}\delta_{jl} + \delta_{il}\delta_{jk}) - \frac{\nu}{1+\nu}\delta_{ij}\delta_{kl}\right\} \tag{3}$$

where G is the shear modulus, ν is Poisson's ratio and $\delta_{ij} = 1$, if $i = j$, but $\delta_{ij} = 0$, if $i \neq j$. The inelastic strain increments have the form

$$d\varepsilon^p_{ij} = \frac{1}{H} P_{ij} Q_{kl} d\sigma_{kl} \tag{4}$$

where H is a hardening modulus, P_{ij} gives the direction of the inelastic strain increment (in stress space), and Q_{kl} is the direction of the normal to the yield surface. If the dependence of the yield surface on stress is given by

$$F(\sigma_{ij}) = 0 \tag{5}$$

where other parameters that keep track of the current state of inelastic deformation are suppressed, then

$$Q_{ij} = \partial F / \partial \sigma_{ij} \tag{6}$$

If a plastic potential exists and is of the form

$$G(\sigma_{ij}) = 0 \tag{7}$$

then

$$P_{ij} = \partial G / \partial \sigma_{ij} \tag{8}$$

If $P_{ij} = Q_{ij}$, then the inelastic strain increment is normal to the yield surface in stress space and the flow rule (or plastic potential) is said to be associated. For rocks (and soils and other geomaterials), observations generally indicate that the traces of P_{ij} and Q_{ij} are not equal, i.e., $P_{kk} \neq Q_{kk}$, and these macroscopic observations are supported by the nature of the microstructural mechanisms of inelasticity, such as frictional sliding and local tensile microcracking due to grain scale inhomogeneities. There appears, however, to be no evidence for deviations from normality in the deviatoric plane (Π - plane or planes in which σ_{kk} is constant). Because there is also no reason to expect such deviations on the basis of microstructural mechanisms, we assume here that $P'_{ij} = Q'_{ij}$, where the prime denotes the deviatoric part of the tensor.

3 Predictions for Two Invariant Model

If the yield function (5) and plastic potential (7) depend on only the first two invariants of the stress, taken to be $\sigma = \sigma_{kk}$ and

$$\tau = (s_{kl}s_{kl}/2)^{1/2} \tag{9}$$

where $s_{ij} = \sigma_{ij} - (\sigma_{kk}/3)\delta_{ij}$ is the deviatoric part of the stress, they can be written as

$$\tau = f(\sigma) \tag{10}$$

and

$$\tau = g(\sigma) \tag{11}$$

Then Q_{ij} (6)and P_{ij} (8) are given by

$$Q_{ij} = \frac{s_{ij}}{2\tau} + \frac{1}{3}\mu\delta_{ij} \tag{12}$$

and

$$P_{ij} = \frac{s_{ij}}{2\tau} + \frac{1}{3}\beta\delta_{ij} \tag{13}$$

where $\mu = -3f'(\sigma)$ is a friction coefficient and $\beta = -3g'(\sigma)$ is a dilatancy factor. For this case $P'_{ij} = Q'_{ij} = s_{ij}/2\tau$.

Extending seminal work by Hadamard [8], Thomas [39], Mandl [18] and Hill [12], Rudnicki and Rice [33] analyzed localization as a bifurcation from homogeneous deformation for the case of a constitutive relation having the form of (4) with (12) and (13). They show the prediction for the angle between normal to the band of localization and the least (most compressive) principal stress is ([33], eqn. (19))

$$\tan^2\theta_{RR} = \frac{\xi - (s_3/\tau)}{(s_1/\tau) - \xi} \tag{14}$$

where

$$\xi = \frac{1}{3}(1+\nu)(\beta+\mu) - (s_2/\tau)(1-\nu) \tag{15}$$

and $s_1 \geq s_2 \geq s_3$ are the largest, intermediate and smallest principal values of s_{ij} (Rudnicki and Rice [33] use $N_{\max}$, N and $N_{\min}$ for s_1/τ, s_2/τ and s_3/τ). Rudnicki and Olsson ([32], eqns. (10) and (11)) rewrite this result in the form

$$\theta_{RR} = \frac{\pi}{4} + \frac{1}{2}\arcsin\alpha \tag{16}$$

where

$$\alpha = \frac{(2/3)(1+\nu)(\beta+\mu) - (s_2/\tau)(1-2\nu)}{\sqrt{4 - 3(s_2/\tau)^2}} \tag{17}$$

For $\alpha \leq -1$, the plane of localization is perpendicular to the most compressive stress ($\theta_{RR} = 0$) and said to be a compaction band. For $\alpha \geq 1$, the plane of localization is perpendicular to the least compressive stress ($\theta_{RR} = \pi/2$) and said to be a dilation band. Observations of compaction bands in porous sandstones in the field ([36], [34]) and in the laboratory ([25], [1], [16], [38], [41], [40], [6], [26], [7]) have been reported recently. Understanding the conditions for their formation and evolution is of interest because they dramatically reduce the permeability for flow across them ([41], [13], [37], [35]). Consequently, their formation in porous subsurface reservoirs could significantly affect applications involving fluid injection or withdrawal. Du Bernard et al. [2] have reported an observation of dilation bands in the field, but they appear to be much less common.

4 Three Invariant Results

Rice [30] has given a more general localization analysis of the constitutive relation (4) without specific reference to the forms of P_{ij} and Q_{ij} and Ottosen and Runesson [28] have extended the analysis for a yield function and plastic potential that depend on all three stress invariants. The results for a three invariant model can, however, be obtained by appropriate replacements in the results of [33].

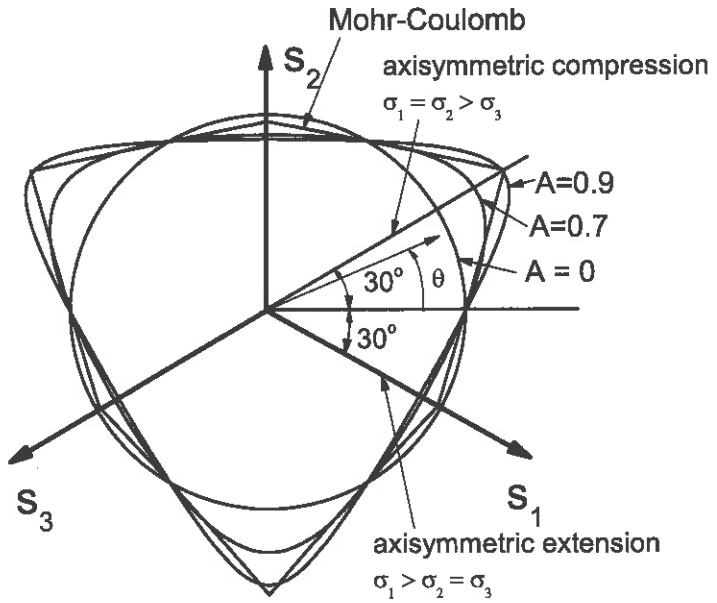

Fig. 1 The figure compares the shape (33) in a the deviatoric plane (σ_{kk} = constant) with the Mohr-Coulomb hexagon. Also shown is the angle θ defined by (18). The axes of the principal deviatoric stresses differ by angles of 120° in this plane.

Two of the invariants are taken to be the trace of the stress $\sigma = \sigma_{kk}$, and the second invariant of the deviatoric stress (or Mises equivalent stress) (9). It is convenient to take the third invariant as the Lode angle [11]

$$\theta = -\frac{1}{3}\arcsin\left(\sqrt{\frac{27}{4}}\frac{J_3}{\tau^3}\right) \tag{18}$$

where $J_3 = \det(s_{ij})$ is the third invariant of the deviatoric stress. Geometrically, the angle (18) defines a 60° sector in planes σ_{kk} =constant, $-\pi/6 \leq \theta \leq \pi/6$ (Figure 1). The limiting values correspond to axisymmetric extension ($\theta = -\pi/6$; $\sigma_1 > \sigma_2 = \sigma_3$) and axisymmetric compression

($\theta = \pi/6$; $\sigma_1 = \sigma_2 > \sigma_3$). Deviatoric pure shear ($\sigma_2 = (\sigma_1 + \sigma_3)/2$) corresponds to $\theta = 0$. Because this angle (18) is related to s_2/τ in (17) by

$$s_2/\tau = 2\sin\theta/\sqrt{3} \tag{19}$$

the result (17) does depend on the third invariant of stress although the yield function and plastic potential on which it is based do not. With this choice of invariants, the yield function and plastic potential have the forms

$$F(\tau, \sigma, \theta) = 0 \tag{20}$$

and

$$G(\tau, \sigma, \theta) = 0 \tag{21}$$

The normal to the yield surface (6) is

$$Q_{ij} = \frac{\partial G}{\partial \sigma_{ij}} = G_\tau \frac{\partial \tau}{\partial \sigma_{ij}} + G_\sigma \frac{\partial \sigma}{\partial \sigma_{ij}} + G_\theta \frac{\partial \theta}{\partial \sigma_{ij}} \tag{22}$$

where the subscript denotes the partial derviative of G with respect to that argument. The derivatives of the first two invariants with respect to stress are easily calculated as $\partial\tau/\partial\sigma_{ij} = s_{ij}/\tau$ and $\partial\sigma/\partial\sigma_{ij} = \delta_{ij}$ and the third is given by

$$\frac{\partial J_3}{\partial \sigma_{ij}} = t_{ij} = s_{ik}s_{kj} - (2/3)\delta_{ij}\tau^2 \tag{23}$$

The tensor t_{ij} is deviatoric ($t_{kk} = 0$) and has the same principal axes as s_{ij}. The result (23) can be used to shown that

$$\frac{\partial \theta}{\partial \sigma_{ij}} = -\frac{1}{\tau}\left\{\frac{\sqrt{3}}{2\cos(3\theta)}\frac{t_{ij}}{\tau^2} + \tan(3\theta)\frac{s_{ij}}{2\tau}\right\} \tag{24}$$

and (22) can be rewritten as

$$Q_{ij} = F_\sigma \delta_{ij} + F_\tau \frac{s_{ij}}{2\tau} - F_\theta \frac{1}{\tau}\left\{\frac{\sqrt{3}}{2\cos(3\theta)}\frac{t_{ij}}{\tau^2} + \tan(3\theta)\frac{s_{ij}}{2\tau}\right\} \tag{25}$$

where the last two terms give the deviatoric part. The direction of the inelastic strain increment is given by the same expression with F replaced by G. The assumption that the deviatoric parts of P_{ij} and Q_{ij} be equal, $Q'_{ij} = P'_{ij}$, requires that

$$F_\tau = G_\tau, \; F_\theta = G_\theta \tag{26}$$

Consequently, the yield function and plastic potential can differ only by a function of σ. Calculating $2Q'_{ij}Q'_{ij}$ yields

$$2Q'_{ij}Q'_{ij} = F_\tau^2 + (F_\theta/\tau)^2 \tag{27}$$

using the intermediate results

$$t_{ij}t_{ij} = 2\tau^4/3$$

and

$$t_{ij}s_{ij} = -2\tau^3\sin(3\theta)/\sqrt{3}$$

5 Expression for the Band Angle

For the three invariant constitutive model and $P'_{ij} = Q'_{ij}$, the band angle is given by the same expressions, (14), (15), (16) and (17), with the replacements:

$$\beta \to \frac{1}{2}\frac{P_{kk}}{\sqrt{Q'_{ij}Q'_{ij}/2}}$$

$$\mu \to \frac{1}{2}\frac{Q_{kk}}{\sqrt{Q'_{ij}Q'_{ij}/2}}$$

$$N_{ij} = \frac{s_{ij}}{\tau} \to \frac{Q'_{ij}}{\sqrt{Q'_{kl}Q'_{kl}/2}}$$

Thus, the expression for α becomes

$$\alpha = \frac{(1/3)(1+\nu)(P_{kk} + Q_{kk}) - Q'_2(1-2\nu)}{\sqrt{2Q'_{kl}Q'_{kl} - 3(Q'_2)^2}} \tag{28}$$

Using (19), (23), (25) and (27) yields the following more compact result:

$$\alpha = \frac{\sqrt{3}(1+\nu)\cos\phi(F_\sigma + G_\sigma) - (1-2\nu)\sin(\phi+\theta)F_\tau}{\sqrt{3}F_\tau\cos(\phi+\theta)} \tag{29}$$

where ϕ, defined by

$$\tan\phi = \frac{F_\theta/\tau}{F_\tau} \tag{30}$$

is the angle between the normal to the yield surface in the deviatoric plane and a radial vector.

5.1 Mohr-Coulomb Result

A number of three invariant yield surfaces have been suggested for soils, rock and concrete (see, e.g., [27], [15], [4]). Of this class, the most familiar, at least in geomechanics, is the Mohr-Coulomb form. Although this condition is usually applied as a failure criterion ([14], [29]), it has also been used for yield (e.g., [23]). The Mohr-Columb condition has the form

$$F_{MC} = q + M(p) = 0 \tag{31}$$

where $q = (\sigma_1 - \sigma_3)/2$ and $p = (\sigma_1 + \sigma_3)/2$. Thus, it does not depend at all on the intermediate principal stress σ_2. Although (31) can be expressed in terms of σ, τ, and θ, it is more convenient to follow [28] and identify the principal values of Q_i directly. The denominator of (28) is unity and (28) reduces to

$$\alpha = (1+\nu)(P_{kk} + M')/3 + (1-2\nu)M'/3 \tag{32}$$

where M' denotes the derivative with respect to its argument. Assuming normality, $P_{kk} = Q_{kk} = M'$ reduces (32) to $\alpha = M'$. Thus, as noted by [28], (32) reduces to the usual Mohr-Coulumb prediction for a friction angle defined by $\arcsin(M')$. Although this result can be used to interpret data from axisymmetric compression, the absence of any dependence on σ_2 is at odds with observations in true triaxial tests ([21], [22], [9], [5], [10], [24]).

6 A Class of Three Invariant Yield Surfaces

A class of three invariant yield surfaces is defined by

$$F(\tau, \sigma, \theta) = -\sqrt{\frac{4}{27}} A \sin(3\theta) \left(\frac{\tau}{\tau_0}\right)^3 + \left(\frac{\tau}{\tau_0}\right)^2 - 1 = 0 \tag{33}$$

where $0 \leq A \leq 1$, and both A and τ_0 may depend on σ. For $A = 0$ and $\tau_0 = \tau_0(\sigma)$, (33) reduces to the form considered by [33] (10). For $A = 1$, the shape of the yield surface in the deviatoric plane is triangular, as for a Rankine material in which yield occurs at a particular value of the largest (least compressive) principal stress. For $\theta = 0$, the first term in (33) vanishes and the condition again reduces to $\tau = \tau_0(\sigma)$. Thus, $\tau_0(\sigma)$ is determined by the mean stress dependence in deviatoric pure shear.

The form (33) has the same shape in the deviatoric plane as the Lade-Duncan ([17], [4]) and Matsuoka-Nakai ([19], [4]) criteria but the mean stress dependence is not specific and can be adjusted by the forms of A and τ_0. In particular, taking

$$\tau_0 = -\frac{\sigma}{3}\sqrt{\frac{(k_{LD} - 27)}{k_{LD}}} \tag{34}$$

and $A = \sqrt{1 - 27/k_{LD}}$ gives the form of the Lade-Duncan criterion in which $k_{LD} > 27$. Taking

$$\tau_0 = -\frac{\sigma}{3}\sqrt{\frac{k_{MN} - 9}{k_{MN} - 3}} \tag{35}$$

and $A = \sqrt{3k_{MN}^2(k_{MN} - 9)/(k_{MN} - 3)^3}$ gives the form of the Matsuoka-Nakai criterion in which $k_{MN} > 9$. Because these two criteria and (33) have the identical shape in the deviatoric plane if normalized to agree in pure shear ($\theta = 0$), the demonstration of convexity by [15] for Lade-Duncan and Matsuoka-Nakai also applies to (33). An advantage of the form (33) is that the dependence of τ_0 and A on σ can be chosen to agree with particular data sets. Figure 1 compares the shape of Mohr Coulomb criterion in the deviatoric plane with the shape of (33) for $A = 0, 0.7$ and 0.9 with all normalized to agree in pure shear. The curve for $A = 0$ is identical with the Mises circle in this plane. For each criterion (except with $A = 0$) the yield stresses differ in axisymmetric compression ($\theta = 30^o$) and axisymmetric extension ($\theta = -30^o$) and the amount of the difference varies for each criterion.

7 Westerly Granite Data

In this section, (33) is used with (29) to model band angle data on Westerly granite. These data combine results of Mogi [20] for axially symmetric extension and compression with more recent true triaxial data of [10]. Rudnicki [31] has examined this data set using (16) and (17) but allowing the sum of $\mu + \beta$ to depend on the mean stress in a manner inferred from the results of axisymmetric compression. Although this analysis roughly captures some trends in the data, the quantitative agreement is not very good. As will be shown here, the use of the three invariant model (33) yields better agreement between data and predictions.

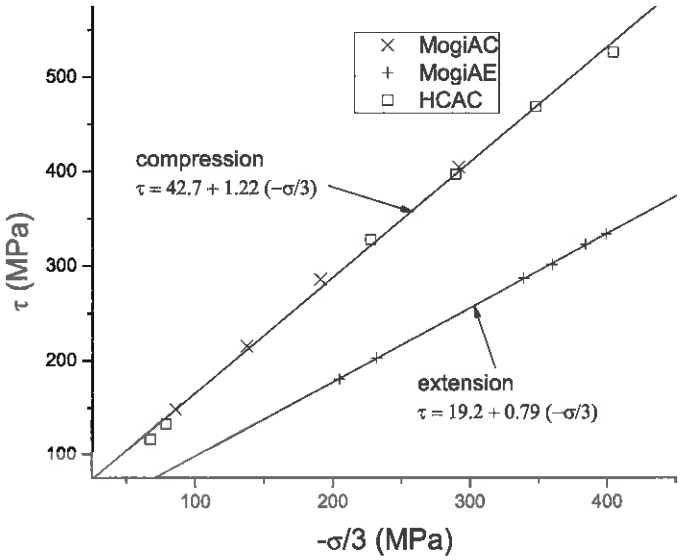

Fig. 2 A plot of τ (at failure) vs. mean normal stress $-\sigma/3$ for the axisymmetric compression and extension tests of [20] and the true triaxial tests of [10] loaded in axially symmetric compression. Also shown are lines fit to the results in compression and extension.

As mentioned earlier, data on the evolution of the yield surface is seldom available for rocks. The data used here are for "failure" which corresponds roughly to the development of a through going fault approximately at a peak in the stress vs. strain curve. As also noted earlier, the bifurcation analysis predicts that localization can occur slightly before peak, for deformation states near plane strain, or well after peak, for axisymmetric deformation states. Although there is some evidence consistent with these predictions [3], localization is typically observed to occur near peak stress. Whether it is

observed slightly before or after depends not only on the deformation state but on a variety of experimental factors such as effective stiffness of the loading machine, nominal deformation rate, precise alignment of the platens and degree of constraint imposed by the end conditions. In the absence of detailed information on yield, I assume the failure data approximately reflect variation of the yield surface. Figure 2 plots τ (at failure) vs. mean compressive stress, $-\sigma/3$, for the axisymmetric extension and compression tests of Mogi [20] on Westerly granite. Also shown are results of Haimson and Chang [10] in a true triaxial apparatus for axisymmetric compression stress states ($\sigma_1 = \sigma_2 > \sigma_3$). Agreement of the tests of [20] and [10] illustrates the consistency of results obtained using the different apparati. The results for both tests are well-modelled by the straight lines given on the graph. The different lines for compression and extension indicate a dependence on the Lode angle θ [31]. For axisymmetric compression, τ is given by $t_{AC}\tau_0(\sigma)$, where t_{AC} is the root of (33) for $\theta = \pi/6$. Similarly, for axisymmetric extension, $\tau = t_{AE}\tau_0(\sigma)$, where t_{AE} is the root of (33) for $\theta = -\pi/6$. The linear variations suggest that it suffices to take A as constant (not dependent on mean stress) and $\tau_0(\sigma)$ as linear:

$$\tau_0(\sigma) = \tau_{00} + \tau_{01}(-\sigma/3) \tag{36}$$

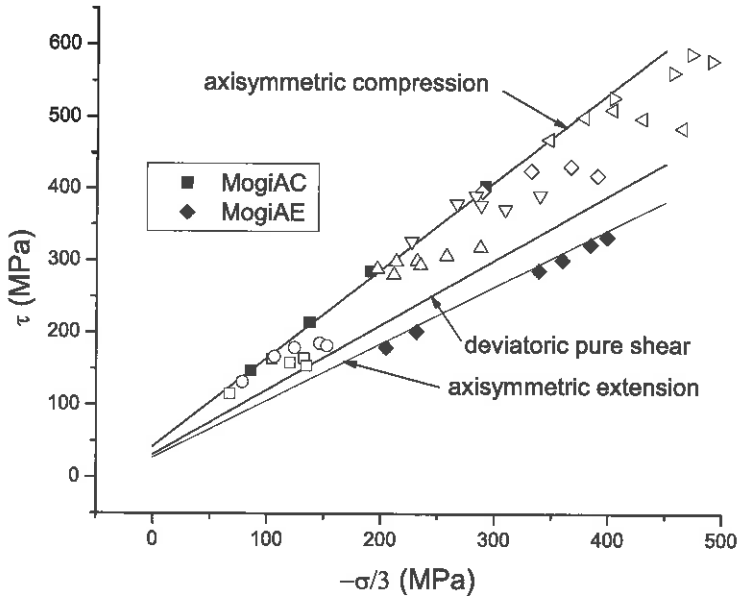

Fig. 3 Plot of τ vs. $-\sigma/3$ for axisymmetric compression and extension data of [20] and all the true triaxial data of [10]. Lines are predictions of (33) for $A = 0.88$ and $\theta = \pi/6$, 0, and $-\pi/6$.

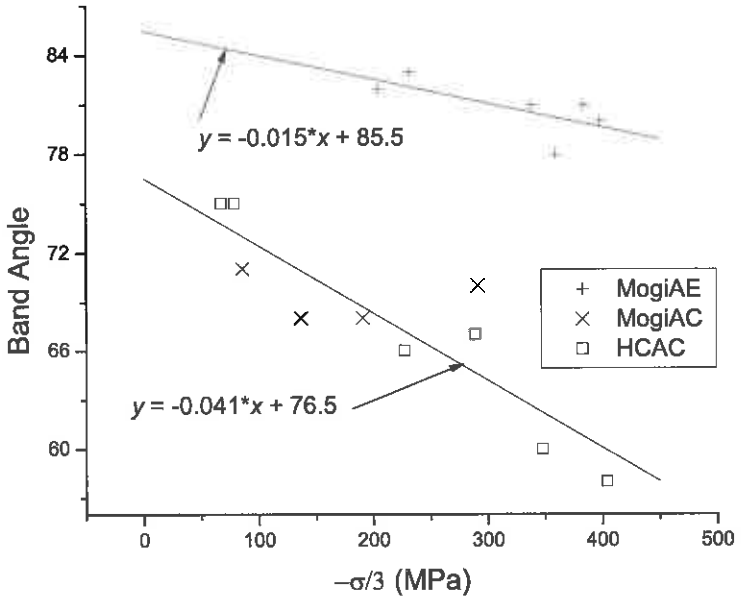

Fig. 4 Measured band angles for axisymmetric compression and extension versus the mean normal stress and straightline fits to the data

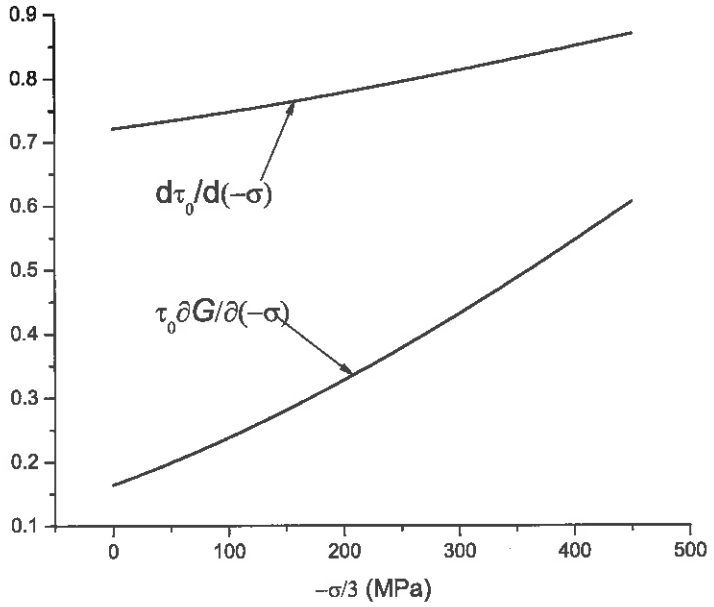

Fig. 5 Variations of $d\tau_0/d\sigma$ and $\tau_0\partial G/\partial\sigma$ inferred from (29) applied to the linear variation of band angles in compression and extension (Figure 4). Vertical axis gives numerical values for both $d\tau_0/d\sigma$ and $\tau_0\partial G/\partial\sigma$.

where τ_{00} and τ_{01} are the intercept and slope of the fit to the axisymmetric compression data in Figure 2 divided by t_{AC}. The value of $A = 0.88$ is chosen so that the ratio of t_{AC}/t_{AE} is equal to the ratio of slopes in Figure 2.

Figure 3 plots the data of [20] shown in Figure 2 along with all the true triaxial data of [10]. The true triaxial tests were conducted by loading the specimens in hydrostatic compression to the level of σ_1, then loading biaxially with $\sigma_2 = \sigma_3$ to a fixed value of σ_2, and finally increasing σ_3 to failure. Different symbols correspond to tests at different values of the least compressive stress (σ_1). From a conceptual point-of-view, it would be preferable to conduct tests at constant values of σ or θ, but both vary during these tests. The lines in Figure 3 show the resulting predictions for axisymmetric compression, axisymmetric extension and deviatoric pure shear from (33) with $A = 0.88$ and (36). Although $\tau_0(\sigma)$ (36) is fixed by the data for axisymmetric compression and A is chosen to give the observed ratio of slopes in compression and extension, the intercept for extension is only slightly larger than that given by the fit to the data; i.e., axisymmetric extension points lie slightly below the line in Figure 2. Furthermore, the values of θ for the true

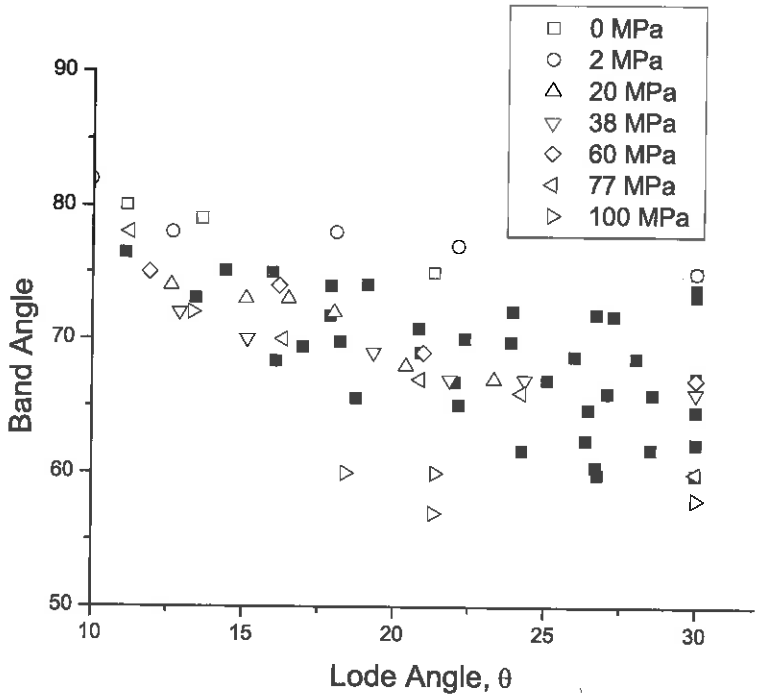

Fig. 6 Comparison of predicted (solid squares) and observed band angles (open symbols) as a function of the Lode angle θ. Different open symbols correspond to the value (shown in legend) of the fixed minimum compressive stress in the test.

triaxial tests lie between 0.0 and 30° which is consistent with the position of the line for deviatoric pure shear. (See Figure 3 of [31] which shows data for the band angle plotted against $2\sin\theta$).

Figure 4 shows the measured band angles for axisymmetric compression and extension versus the mean normal stress and straightline fits to the data. The derivatives F_τ and F_θ that enter (29) and (30) can easily be calculated from (33). If A is a constant and only τ_0 depends on σ, then

$$F_\sigma = \frac{1}{\tau_0}\frac{d\tau_0}{d\sigma}\left[\left(\frac{\tau}{\tau_0}\right)^2 - 3\right] \tag{37}$$

where the ratio τ/τ_0 depends on θ for a given value of A. $G_\sigma$in (29) is unknown but can be determined along with $d\tau_0/d\sigma$ from the observed variations of the band angles in axisymmetric compression and extension. In other words, using the linear fits to the band angle data shown in Figure 4 in the expressions (16) with (29) and (30) evaluated for compression and extension yields two linear equations to determine G_σ and $d\tau_0/d\sigma$. The results are shown in Figure 5. The inferred dependence of $d\tau_0/d\sigma$ with σ is not consistent with the linear variation of $\tau_0(\sigma)$ shown in Figure 2. Nevertheless, the variation of $d\tau_0/d\sigma$ is small (0.72 to 0.87) and only slightly below the value used to plot the lines in Figure 2 (0.898). This discrepancy may be due to the issues discussed earlier

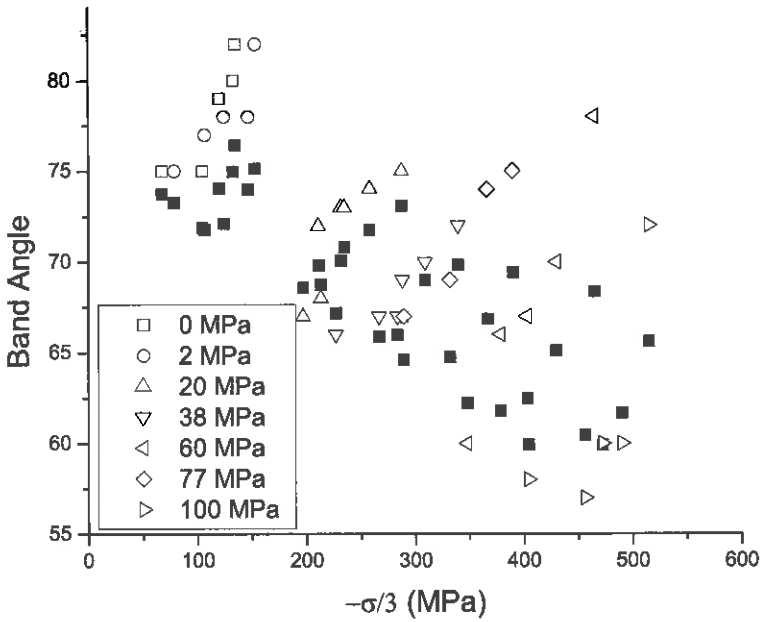

Fig. 7 Same as Figure 6 but plotted against the mean normal compressive stress $-\sigma/3$

about using failure data to approximate the variation of the yield surface. The data for stress at failure are, however, only used to estimate the value of A. Alternatively, the value of A could be chosen to improve the agreement between the predictions and observations of the band angle data.

Figure 6 compares the values of the predicted and observed band angles as a function of the Lode angle θ. The agreement is good and the correlation between the two data sets is 0.912. Figure 7 shows the comparison as a function of mean stress. Note that the predictions capture the roughly linear increase in band angle with increasing intermediate principal stress and the generally downward trend with increasing mean compressive stress.

8 Conclusion

Data from true triaxial tests provide an opportunity to investigate the form of three-dimensional constitutive relations for rocks. Tests at multiple mean stresses for axisymmetric compression and extension can be used to infer the behaviour for other deviatoric stress states and mean stresses. Use of the predictions for the band angle from bifurcation theory with a simple form of the yield function that depends on all three stress invariants yields results that are an improvement over those based on the two invariant model. The predictions are in reasonable agreement with the observations on Westerly granite and it will be interesting to see if similarly good agreement can be achieved with other rock types.

Acknowledgement. I am grateful to Bezalel Haimson for providing me with his experimental data and for many helpful discussions. I also greatly appreciate the many discussions with Florent Gimbert about three invariant constitutive models. Partial financial support for this work was provided by the US Department of Energy, Office of Science, Basic Energy Sciences, Geosciences program through grant DE-FG02-93ER14344/A016 to Northwestern University.

References

[1] Baud, P., Klein, E., Wong, T.-F.: Compaction localization in porous sandstones: Spatial evolution of damage and acoustic emission activity. Journal of Structural Geology 26, 603–624 (2004)

[2] Bernard, X.D., Eichhubl, P., Aydin, A.: Dilation bands: A new form of localized failure in granular media. Geophysical Research Letters 29(24), 2176 (2002), doi:10.1029/2002GL015966

[3] Bésuelle, P., Rudnicki, J.W.: Localization: Shear bands and compaction bands. In: Guéguen, Y., Boutéca, M. (eds.) Mechanics of Fluid Saturated Rocks. International Geophysics Series, vol. 89, pp. 219–321. Academic Press, London (2004)

[4] Borja, R.I., Sama, K.M., Sanz, P.F.: On the numerical integration of three-invariant elastoplastic constitutive models. Computer Methods in Applied Mechanics and Engineering 192, 1227–1258 (2003), doi:10.1016/S0045-7825(02)00620-5

[5] Chang, C., Haimson, B.: True triaxial stength and defomrability of the german continental deep drilling program (KTB) deep hole amphibolite. Journal of Geophysical Research 105(B8), 999–919 (2000)

[6] DiGiovanni, A.A., Fredrich, J.T., Holcomb, D.J., Olsson, W.A.: Micromechanics of compaction in an analogue reservoir sandstone. In: Girard, J., Liebman, M., Breeds, C., Doe, T. (eds.) Pacific Rocks 2000, Proceedings of the 4th North American Rock Mechanics Symposium, pp. 1153–1158. A. A. Balkema (2000)

[7] Fôrtin, J., Stanchits, S., Dresen, G., Guéguen, Y.: Acoustic emission and velocities associated with the formation of compaction bands in sandstone. Journal of Geophysical Research 111(B10203) (2006), doi:10.1029/2005JB003854

[8] Hadamard, J.: Leçons sur la Propagation de Ondes et Les Equations de L'Hydrodynamique, Paris (1903)

[9] Haimson, B.: True triaxial stresses and the brittle fracture of rock. Pure and Applied Geophysics 163, 1101–1130 (2006), doi: 10.007/s00024-006-0065-7

[10] Haimson, B., Chang, C.: A new true triaxial cell for testing mechanical properties of rock, and its use to determine rock strength and deformability of Westerly granite. International Journal of Rock Mechanics and Mining Science 37(1-2), 285–296 (2000)

[11] Hill, R.: The Mathematical Theory of Plasticity. Oxford Engineering Science Series, Oxford, London (1950)

[12] Hill, R.: Acceleration waves in solids. Journal of the Mechanics and Physics of Solids 10, 1–16 (1962)

[13] Holcomb, D.J., Olsson, W.A.: Compaction localization and fluid flow. Journal of Geophysical Research 108(B6, 2290) (2003), doi: 10.1029/2001JB000813

[14] Jaeger, J.C., Cook, N.G.W.: Fundamentals of Rock Mechanics. John Wiley and Sons, Inc., New York (1969)

[15] Jiang, J., Pietruszczak, S.: Convexity of yield loci for pressure sensitive materials. Computers and Geotechnics, 51–63 (1988)

[16] Klein, E., Baud, P., Reuschlé, T., Wong, T.-F.: Mechanical behaviour and failure mode of Bentheim sandstone under triaxial compression. Physics and Chemistry of the Earth (A) 26, 21–25 (2001)

[17] Lade, P.V., Duncan, J.M.: Elastoplastic stress-strain theory for cohesioness soil. J. Geotech. Engrg. Div., ASCE 101, 1037–1053 (1975)

[18] Mandel, J.: Conditions de stabilté et postulat de drucker. In: Kravtchenko, J., Sirieys, P.M. (eds.) Rheology and Soil Mechanics, pp. 58–68. Springer (1966)

[19] Matsuoka, H., Nakai, T.: Stress-deformation and strength characteristics of soil under three different principal stresses. Proc. Japan Soc. Civil Engn., 1037–1053 (1974)

[20] Mogi, K.: Effect of the intermediate principal stress on rock failure. Journal of Geophysical Research 72, 5117–5131 (1967)

[21] Mogi, K.: Effect of the triaxial stress system on the failure of dolomite and limstone. Tectonophysics 11, 111–127 (1971)

[22] Mogi, K.: Experimental Rock Mechanics. Geomechanics Research Series, vol. 3.Taylor & Francis (2007)

[23] Molenkamp, F.: Comparison of frictional material models with respect to shear band initiation. Géotechnique 35(2), 127–143 (1985)
[24] Oku, H., Haimson, B., Song, S.-R.: True triaxial strength and deformability of the siltstone overlying the chelungpu fault (chi-chi earthquake), taiwan. Geophysical Research Letters 34(L09306) (2007), doi:10.1029/2007GLO29601
[25] Olsson, W.A.: Theoretical and experimental investigation of compaction bands. Journal of Geophysical Research 104, 7219–7228 (1999)
[26] Olsson, W.A., Holcomb, D.J.: Compaction localization in porous rock. Geophysical Research Letters 27(21), 3537–3540 (2000)
[27] Ottosen, N.S.: Theoretical framework for modelling the behaviour of frictional materials. International Journal of Solids and Structures 22(11), 1325–1342 (1986)
[28] Ottosen, N.S., Runesson, K.: Properties of discontinuous bifurcation solutions in elasto-plasticity. International Journal of Solids and Structures 27, 401–421 (1991)
[29] Paterson, M.S., Wong, T.-F.: Experimental Rock Deformation - The Brittle Field, 2nd edn. Springer, Heidelberg (2005)
[30] Rice, J.R.: The localization of plastic deformation. In: Koiter, W.T. (ed.) Proceedings of the 14th International Congress on Theoretical and Applied Mechanics Theoretical and Applied Mechanics, pp. 207–220. North-Holland Publishing Company, Delft (1976)
[31] Rudnicki, J.W.: Localized Failure in Brittle Rock. In: Proceedings of the 3rd International Symposium GeoProc 2008, pp. 25–40. Wiley (2008)
[32] Rudnicki, J.W., Olsson, W.A.: Reexamination of fault angles predicted by shear localization theory. International Journal of Rock Mechanics and Mining Science 35, 512–513 (1998); extended abstract, full paper on CD Rom.
[33] Rudnicki, J.W., Rice, J.R.: Conditions for the localization of deformation in pressure-sensitive dilatant materials. Journal of the Mechanics and Physics of Solids 23, 371–394 (1975)
[34] Sternlof, K.R.: Structural geology, propagation mechanics and hydraulic effects of compaction bands in sandstone, Ph.D. thesis, Stanford University (2006)
[35] Sternlof, K.R., Chapin, J.R., Pollard, D.D., Durlofsky, L.J.: Permeability effects of deformation band arrays in sandstone. American Association of Petroleum Geologists Bulletin 88, 1315–1329 (2004)
[36] Sternlof, K.R., Rudnicki, J.W., Pollard, D.D.: Anti-crack inclusion model for compaction bands in sandstone. Journal of Geophysical Research 110(B11403) (2005), doi:10.1029/2005JB003764
[37] Sternlof, K.R., Karimi-Fard, M., Pollard, D.D., Durlofsky, L.J.: Flow effects of compaction bands in sandstone at scales relevant to aquifer and reservoir management. Water Resources Research 42(W07425) (2006), doi:10.1029/2005WR004664
[38] Tembe, S., Vajdova, V., Wong, T.-F., Zhu, W.: Initiation and propagation of strain localization in circumferentially notched samples of two porous sandstones. Journal of Geophysical Research 111(B02409) (2006), doi:10.1029/2005JB003611
[39] Thomas, T.Y.: Plastic Flow and Fracture in Solids. Academic Press (1961)

[40] Vajdova, V., Wong, T.-F.: Incremental propagation of discrete compaction bands and microstructural observations on circumferentially notched samples of Bentheim sandstone. Geophysical Research Letters 30(14), 1775 (2003), doi:10.1029/2003GL017750.
[41] Vajdova, V., Baud, P., Wong, T.-F.: Permeability evolution during localized deformation in Bentheim sandstone. Journal of Geophysical Research 109(B10406) (2004), doi:10.1029/2003JB002942
[42] Wawersik, W.R., et al.: Terrestrial sequestration of CO2: An assessment of research needs. In: Dmowska, R. (ed.) Advances in Geophysics, vol. 43, pp. 97–177. Academic Press (2001)